Polarization of Recoil Protons from Electron-Proton Scattering at 950 MeV

J. C. Bizot, J. M. Buon, J. Lefrançois, J. Perez-y-Jorba, and P. Roy
Ecole Normale Supérieure, Laboratoire de l'Accélérateur Linéaire, Orsay (Seine-et-Oise), France
(Received 7 July 1965)

The recoil-proton polarization in elastic high-energy electron scattering on protons has been measured in order to check the validity of first Born approximation in this reaction. The transverse polarization is proportional to the imaginary part of the second order term (two-photon exchange term). 950-MeV electrons produced by the Orsay Linear Accelerator were scattered in a liquid-hydrogen target at about 90° c.m. The recoil protons were analyzed by a magnet system. Their polarization was then measured in a polarimeter constituted by a carbon scatterer and 4 spark chambers. The two transverse components of the polarization have been calculated by a method derived from maximum likelihood. The component perpendicular to the scattering plane was found to be 0.040 ± 0.027. The transverse component in the scattering plane was found to be $0.000+0.028$.

I. INTRODUCTION

A. The Two-Photon Exchange Term

So far electron-nucleon scattering has been analyzed using the Rosenbluth formula[1] for the elastic cross section. In this formula it is assumed that only one virtual photon is exchanged between electron and nucleon, as illustrated in Fig. 1. Then the cross section is proportional to $\alpha^2=(e^2/\hbar c)^2$.

As pointed out by Drell and Fubini,[2] the higher order corrections are expected to be small because of the weakness of the electromagnetic coupling constant.

The largest corrections proportional to α^3 would be due to the interference between the one-photon and the two-photon terms. Figure 2 gives the relevant Feynman diagrams with two virtual photons. Among these, $M1$ and $M2$ contribute only to the radiative corrections, which are calculated straightforwardly. On the other hand, $M3$ and $M4$ imply a two-photon exchange between electron and nucleon. They cannot be accurately calculated at large momenta because of the lack of knowledge of mesonic effects. For example, resonances in the BeV region can produce an enhancement of $M3$ and $M4$ amplitude, compensating partially the weakness of the electromagnetic coupling constant.

Experimentally it is extremely interesting to investigate effects due to these two-photon exchange terms. First, they can affect the linear dependence of the cross section on $\tan^2(\theta/2)$, which appears in the Rosenbluth formula when the momentum transfer is held constant and the scattering angle θ is varied. But Gourdin and Martin[3] and Flamm and Kummer[4] pointed out that appreciable departure from the linearity can only occur at small angles θ. Effectively up to now, no deviation has been observed even at small angles.[5,6]

Second, one can try to detect a difference in the cross sections for electron-proton and positron-proton elastic scattering. Here the difference is directly proportional to the real part of the two-photon amplitude. Browman, Liu, and Schaerf[7] obtain for a transfer squared of 19.5 F^{-2} a ratio $n_+/n_-=1.08\pm0.04$.

Third, one can measure the polarization of the recoil proton. This polarization is proportional to the interference between the real part and the imaginary part of the total scattering amplitude, that is, neglecting the higher order terms, to the imaginary part of the two-photon exchange term, since the first-order amplitude is real.

We may notice that the last two methods, unlike the first, give answers directly proportional to the total magnitude of the two-photon effect and then may be considered as more sensitive.

The recoil-proton polarization, owing to the con-

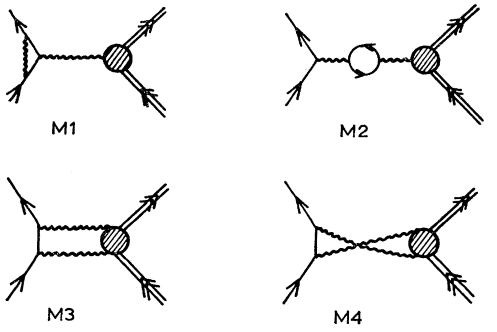

FIG. 2. Second-order Feynman diagram with two virtual photons.

FIG. 1. First-order Feynman diagram.

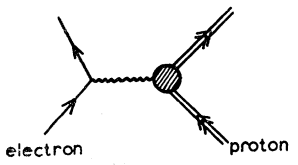

[1] M. N. Rosenbluth, Phys. Rev. **79**, 615 (1950).
[2] S. D. Drell and S. Fubini, Phys. Rev. **113**, 741 (1959).
[3] M. Gourdin and A. Martin, CERN, report, Geneva (unpublished).
[4] D. Flamm and W. Kummer, Nuovo Cimento **28**, 33 (1963).
[5] D. Aitken, R. Hofstadter, E. B. Hughes, T. Jansenss, and M. R. Yearian, in *Proceedings of the International Conference on High-Energy Nuclear Physics at CERN*, edited by J. Prentke (CERN, Geneva, 1962), p. 185.
[6] J. R. Dunning, K. W. Chen, N. F. Ramsey, J. R. Rees, W. Shlaer, J. K. Walker, and R. Wilson, Phys. Rev. Letters **10**, 500 (1963).
[7] A. Browman, F. Liu, and C. Schaerf, Phys. Rev. Letters **12**, 183 (1964).

servation of parity in electromagnetic interactions, must be perpendicular to the scattering plane.

Several authors[2,3,8] have tried to estimate the order of magnitude of the two-photon terms. Guerin and Piketty,[9] using the isobaric model of Gourdin and Salin[10] in order to evaluate the contribution of the virtual Compton effect, have calculated the proton polarization. They found a polarization less than 0.01 for electron energies up to 1 BeV.

B. Accuracy of the Polarization Measurement

From what has just been said, it is seen that the polarization is probably of the order of 0.01 or less, that is, from an experimental point of view, very weak. So, the more accurate the experimental measurement, the more interesting the result.

The accuracy of the measurement relies on two things: the number of analyzed events and the smallness of the systematic errors.

Sixty thousand pictures of the spark chambers have been taken; 20 000 have been retained for trajectory measurements. Finally, 10 000 have been used in the polarization calculation.

We have tried to limit the experimental errors to a 0.01 level. In order to do so, the directions of the trajectories have been measured with an accuracy of 0.05°.

Another cause of error is the uncertainty ΔA on the analyzing power A. The corresponding error on P is given by $\Delta P/P=\Delta A/A$. One sees that if P is weak, it is not necessary to know A with great accuracy. In our case where we used a carbon scatterer, the analyzing power was known to 5%.

C. Choice of Kinematical Parameters

The 950-MeV electrons were scattered at a scattering angle θ c.m.$=91.2°$ corresponding to a transfer $q^2=15.4$ F^{-2}. In this choice two considerations were taken into account:

(1) The recoil proton energy of 324 MeV corresponds to a good value of the analyzing power (about 0.6). For higher proton energies it becomes very weak and one must slow down the protons before analysis which means a loss of counting rate through nuclear interactions.

(2) Two parasitic reactions are associated with the one of interest. They are[11]

$$\gamma+p\rightarrow p+\pi^0,$$
$$e+p\rightarrow e+p+\pi^0.$$

The associated protons are strongly polarized and must then be separated from the elastic protons.[12] In our condition the maximum momentum of these protons is 2% smaller than the elastic one. So, a magnetic separation is then possible. This separation would be more difficult at smaller proton angle or large incident energy.

II. EXPERIMENTAL APPARATUS

A. General

The experimental arrangement is shown in Fig. 3. A 950-MeV electron beam struck a liquid-hydrogen target. The protons recoiling in a horizontal plane at a mean angle $\theta=40.3°$ were momentum-analyzed by a magnetic spectrometer with a 1% resolution. We selected protons in a 1.6% momentum band centered on the elastic peak. These protons entered into a polarimeter where their transverse polarization was measured by letting them scatter in a carbon block. The trajectory of each proton before the carbon block was determined by two spark chambers. In each spark chamber we measured the coordinates of one trajectory point with respect to the laboratory system. Then a trajectory was determined by two points. The two spark chambers were 60 cm apart in order to get an accuracy of 0.05° on the direction. In the same manner the trajectory after the carbon block was determined by two other spark chambers 60 cm apart.

B. The Beam and the Target

We used the electron beam of the Orsay Linear Accelerator in the "1-GeV" target room. Its energy was 950 MeV. A slit in the magnetic deviation system limited the energy dispersion to 1%.

The beam was focused on a liquid hydrogen target of a type designed by Walker *et al.*[13] The beam spot obtained on the target was about 5 mm in diameter. The target cell was 10 cm long, 4 cm wide, 6 cm high; the walls were made of 1 cm brass. The entrance and exit windows were made of 60-μ aluminum. Two pieces of 5-cm brass close to the target cell reduced the counting rate due to protons emitted from these two

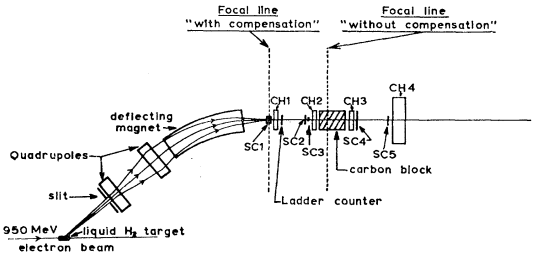

FIG. 3. Experimental setup.

[8] S. D. Drell and M. Ruderman, Phys. Rev. **106**, 561 (1957).
[9] F. Guérin and C. A. Piketty, Nuovo Cimento **32**, 971 (1964).
[10] M. Gourdin and P. Salin, Nuovo Cimento **27**, 193 (1963).
[11] We will discuss later the protons produced by the Compton effect.
[12] R. Querzoli, G. Salvini, and A. Silverman, Nuovo Cimento **19**, 53 (1961).
[13] J. K. Walker, J. P. Burq, and V. Round, Nucl. Instr. Methods **22**, 138 (1963).

windows. The protons scattered at an angle $\theta=40°$ left the target through a third window which limited the useful target length to 4 cm.

A secondary electron monitor was placed behind the target for measuring the beam intensity.

C. The Spectrometer

The spectrometer was made of two quadrupole lenses and a uniform-field bending magnet. The aperture and the length of the quadrupole pole faces were 20 cm and 30 cm, respectively. The maximum field gradient was 1 kG/cm. The length of the bending magnet mean ray was 2.50 cm and its radius of curvature was 4.33 m. The pole gap was 7 cm.

The center of the first quadrupole was 1.8 m away from the target and it was divergent in the horizontal plane. The second quadrupole was convergent in the same plane. With this choice the beam height at the entrance of the bending magnet was small enough to pass through the magnet pole gap. The distance between the two quadrupole centers was 1.35 m and their horizontal focal lengths were -0.9 m and 1.5 m, respectively. The uniform-field magnet bent 845-MeV/c protons horizontally through 42° towards the electron beam. The angle between the pole edges and the central proton trajectory was 7°. Multiple scattering in the spectrometer was reduced by a helium bag.

The spectrometer focal line was 1.6 m behind the exit face of the bending magnet. Kinematically the elastic proton energy varies with its scattering angle, so the momentum resolution on the focal line is limited by the spectrometer horizontal aperture. This aperture was determined by a slit in front of the first quadrupole. For a 1% resolution this aperture must be less than 1 cm. Taking into account this kinematical energy variation, a straightforward first-order calculation shows that elastic-proton trajectories are focused on another focal line, called focal line "with compensation."[14] In our spectrometer this focal line was 0.9 m in front of the ordinary focal line. Thus the momentum resolution on this focal line "with compensation" is independent of the spectrometer horizontal aperture and is the same as for a zero aperture. So we could use a large-aperture slit, 4 cm wide and 12 cm high, in order to increase the counting rate. These slit dimensions are determined so that no proton trajectory hits a magnet pole piece. The momentum resolution obtained on a focal line is also limited by the target magnification. This is another advantage of the focal line "with compensation" where this magnification is rather smaller than on the ordinary focal line, when the former is nearer the magnet exit face. Thus in our spectrometer the target magnification was only 0.11 and we could use a relatively long target length of 4 cm. Finally the spectrometer solid angle was 1.6 msr and the computed dispersion on the focal line "with compensation" was 8×10^{-3} cm^{-1}. The spectrometer design was experimentally checked by the floating-wire method and by measuring the spectrum of protons on the focal line "with compensation" with the help of a small scintillation counter. Figure 4 gives this spectrum and shows that a 1% momentum resolution is achieved; that resolution is sufficient for a good separation of elastic and inelastic protons.

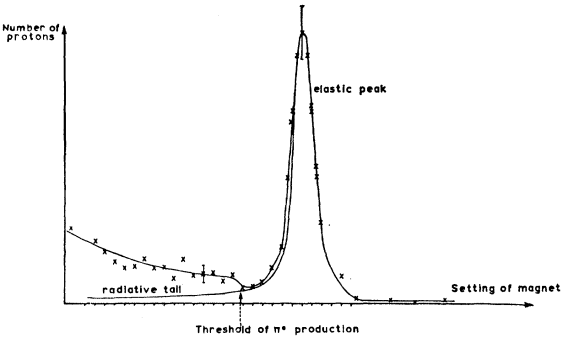

FIG. 4. Proton spectrum on the focal line "with compensation" in a small scintillation counter.

D. The Carbon Scatterer and the Counters

The analyzing scatterer was placed 1.5 m behind the spectrometer, Fig. 3. It was a carbon block 20 cm long, 18 cm wide, and 18 cm high. Passing through this carbon block the protons were slowed down from 300 to 170 MeV.

The protons were detected and the spark chambers triggered by an assembly of 8 scintillation counters. These were made of SPF plastic scintillator connected by light pipes to 56 AVP phototubes. The scintillator dimensions are given in Table I.

TABLE I. Scintillator dimensions.

Counter	Height (cm)	Width (cm)	Thickness (cm)
SC1	7.5	2	0.5
E_1 E_2 E_3	7.5	0.3	0.5
SC2	5	9	1.5
SC3	5	2.5	1.5
SC4	17	17	1.0
SC5	18-cm-diam disc		1.5

Counter SC1 was placed on the focal line "with compensation" and counter SC2 was placed just in front of the second spark chamber CH2. A main coincidence between SC1 and SC2 detected elastic protons in a 1.6% momentum band. A ladder counter made of three small counters E1, E2, E3 was used to center the elastic peak on the 1.6% momentum band. It was placed 10 cm behind the focal line "with compensation."

[14] J. C. Bizot, J. M. Buon, J. Lefrançois, J. Perez-y-Jorba, and P. Roy. Compt. Rend. **260**, 1617 (1965).

Counter SC4, just behind the carbon block, detected the protons leaving the carbon block. Counter SC5, just in front of the big spark chamber CH4, detected protons not scattered in the carbon block. Counter SC3 limited the width of the incident proton beam on the carbon block and prevented some nonscattered protons from passing outside of the counter SC5.

E. The Spark Chambers

Spark chamber CH1 was placed just behind the focal line "with compensation," and spark chamber CH2 in front of the carbon block. Spark chamber CH3 was placed just behind the carbon block and spark chamber CH4 60 cm behind CH3.

CH1, CH2, and CH3 were small 6-gap spark chambers, 17 cm wide and 17 cm high. The plates were made of 1-mm aluminum and were placed in grooves which were milled 5 mm apart in walls of a Lucite box. Two 15-cm-diam windows made of 170-μ Mylar allowed the entrance and the exit of protons. CH4 was a 9-gap spark chamber, 70 cm wide and 70 cm high. In order to perform a range measurement of the protons plates were made of 3-mm aluminum or copper, spaced 1 cm apart. A 6-mm copper plate was placed in front of the chamber. Thus elastic protons were stopped in the chamber plates and the last spark of a proton track gave the stopping plate. The four chambers were filled with a mixture of 99% neon and 1% argon.

Each chamber was photographed on two sides. 8 pictures of the 4 spark chambers were obtained on the same frame (24 mm×36 mm) through an assembly of 16 flat mirrors. The film advance system of the camera was triggered by the same pulse as the spark chambers.

Fiducial marks were drawn on the sides of each spark chamber and were photographed at the same time as the sparks by lighting them with small flash spots.

F. Electronic Circuitry

A block diagram of the electronic circuitry is shown in Fig. 5. The main coincidence 12 between SC1 and SC2 gave the counting rate of elastic protons entering the polarimeter. Three coincidences between each counter of the ladder counter and the main coincidence enabled to center the elastic peak on the polarimeter axis. A coincidence between SC3 and SC4 detected good protons entering and leaving the carbon block. A scattered proton in the carbon block was thus detected by a coincidence 12345, and spark chambers were triggered on that coincidence pulse. We used coincidence circuits of a type designed by Barna *et al.*[15] A blocking circuit prevented the 12345 coincidence pulse from triggering spark chambers during the camera dead time (approximately 1 sec).

The 12345 coincidence pulse triggered four 5C22 thyratron pulsers. Each spark chamber's high-voltage plate was connected to a condenser (1000 pF for CH1, CH2, CH3, and 2000 pF for CH4). The other plates were connected to the ground by small resistors. Each pulser shorted the high-voltage side of the condensers of one spark chamber.

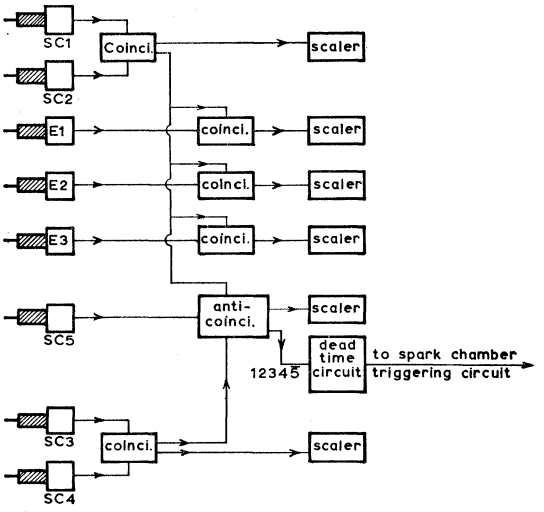

FIG. 5. Block diagram of the electronic circuitry.

G. Shielding

Because of the small duty cycle of the accelerator (3×10^{-5}), a large background was observed around the spark chambers. To reduce this background to a small enough level, thick shielding was needed: The liquid hydrogen target was shielded by 10-cm-thick lead and, behind the target, the electron beam passed inside a helium bag, up to the target room exit. We also shielded the exit of the bending-magnet gap against particles scattered in the pole pieces. The polarimeter was placed in a shelter with 1-m-thick heavy concrete walls and a 30-cm-thick concrete roof. Inelastic protons passing outside the counter SC1 were prevented from entering the spark chambers by stopping them in a 12-cm-thick brass wall around counter SC1. We thus obtained less than one background spark in each gap of the big spark chamber per picture.

III. EXPERIMENTAL PROCEDURE

A. Alignment of the Spark Chambers

In each chamber we choose to measure the coordinates of a point of the particle trajectory located in the median plane of the first gap of the chamber. In order to do so one must measure the coordinates of the corresponding spark with respect to fiducial marks in the spark chamber, and also the coordinates of the fiducial marks of each chamber with respect to the laboratory system.

With the usual small-angle approximation for the

[15] A. Barna *et al.*, Nucl. Instr. Methods **7**, 124 (1960).

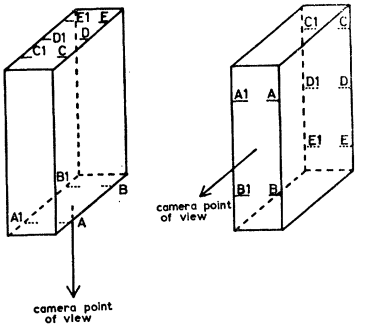

FIG. 6. Fiducial marks drawn on a spark chamber for the two camera points of view.

optical system, the relation between the coordinates x, y of a point in the first-gap median plane and the coordinate x' of its image on one spark-chamber view on the film is of the form

$$x' = (x+\beta y+\gamma)/(\alpha' x+\beta' y+\gamma').$$

The 5 unknown parameters $(\beta, \gamma, \alpha', \beta', \gamma')$ correspond to the position of the optical center of the lens camera (two parameters) and the position of the film plane (3 parameters). To measure these "unknown" parameters one must photograph 5 fiducial marks, located in the first-gap median plane. The position of these marks (ABCDE) is indicated in Fig. 6. Five other marks (A1 B1 C1 D1 E1) in the last-gap median plane allowed us to calculate also the direction of the trajectory in a spark chamber with respect to the AA1 and BB1 lines. The direction obtained in this way is far less precise than the computed direction obtained by measuring the coordinates of two points in two successive spark chambers. Thus we only check the agreement between these two direction determinations.

In theory, once the coefficients β, γ, α', β', γ' have been determined on one photograph for each spark-chamber's view, one needs to measure only one fiducial mark in each view at the same time as the spark track; in practice the 5 marks were photographed about 10 times at the beginning and the end of each film and the result of the measurements averaged. Furthermore, both marks A and B were photographed at the same time as the spark (this allowed us to correct for film stretching).

The position of the fiducial marks of a given chamber with respect to each other was determined accurately with a cathetometer and a high-precision spirit level. The typical error in a series of measurements was of the order of 0.05 mm.

The positions of the chambers with respect to a general laboratory system were determined before and after each run with the help of a theodolite and a cathetometer. The reproducibility of the measurements for lateral or vertical displacement was better than 0.05 mm. Longitudinal distances along the spectrometer axis were measured with a ruler; the errors were thus roughly 5 mm. During these alignments, and during the data-taking runs, the temperature of the chambers was measured in order to correct for thermal expansion of the spark-chamber Lucite boxes.

B. Adjustment of the Electronics

We first adjusted delays in the counters forming the main coincidence 12. A gate circuit was opened with this coincidence and we sent the pulses from each counter, through this gate and a stretcher, to a pulse-height analyzer. We then adjusted the high voltage on each phototube in such a way that no proton signal was lower than the coincidence threshold (1.5 V). We adjusted the delay for each counter in order to form the different coincidences. Since the counters are far less sensitive to general room background than the spark chambers, the amount of shielding we disposed around the apparatus decreased the counter background to an extremely low level. We could thus use a rather large resolving time for the coincidences ($2\tau = 10$ to 20 nsec) and still keep the random coincidences to an extremely small value (less than 0.1%).

The only counter the efficiency of which was critical was SC4; this is due to the fact that particles scattering to the right will pass closer to the SC4 phototube and will give a bigger signal than those scattering to the left. This effect could have caused a false asymmetry, if the efficiency of the SC4 counter had not been 100%, by selecting preferentially events scattered to the right. Inefficiency in counters placed before the carbon block cannot cause such an asymmetry; inefficiency in the anticoincidence counter SC5 would increase the number of scanned events, but again cannot cause false asymmetry since these false events are rejected in the scanning procedure.

During all our runs we have checked permanently the spectrum in counter SC4, Fig. 7, and we estimate that its efficiency was at all times greater than 0.997.

C. Checks on the Proton Beam

The momentum of the proton beam at the focal line "with compensation" is given in Fig. 4. We observed on the high-energy side a relatively uniform background which corresponded roughly to the empty target background of π mesons or protons and probably to a small amount (0.5%) of the so-called "ghost" protons from reactions:

$$\begin{aligned} \gamma + p &\rightarrow \pi^+ + n \\ &\downarrow \\ \pi^+ + p &\rightarrow \pi^+ + p. \end{aligned}$$

Below the elastically scattered proton peak we detected recoil protons from the π^0 electroproduction or photoproduction. From this spectrum, we calculated that the maximum admixture of recoil protons from the π^0 production, in the 1.6% momentum band we used during the data-taking runs, was less than 0.1%. Using the same spectrum and the cross section given by

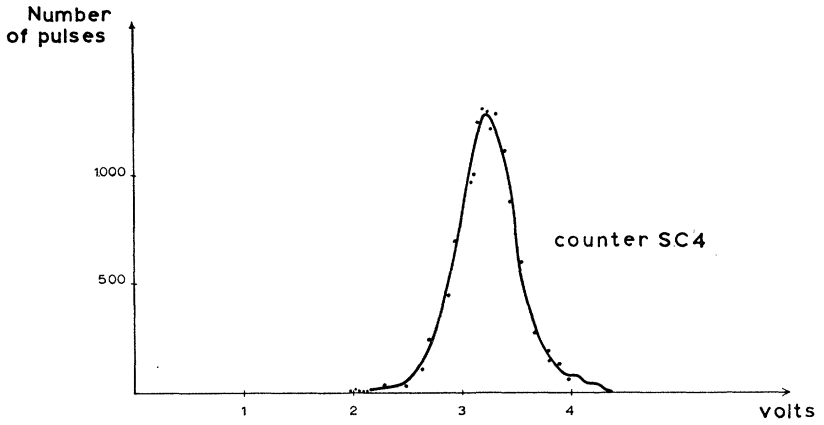

FIG. 7. Pulse spectrum in counter SC4.

Stiening *et al.*[16] we calculated an upper limit of 0.15% on the contamination of recoil protons from Compton scattering:

$$\gamma+p\rightarrow\gamma+p.$$

During the data-taking run we permanently measured the counting rate of the main coincidence 12 and the coincidences between 12 and each of the small counters E1, E2, and E3. This allowed us to keep the elastic peak centered in the 1.6% momentum band determined by SC1 and SC2.

We also measured during our runs the counting rates in the different coincidences. These are listed in Table II.

IV. PICTURE SCANNING AND POLARIZATION COMPUTATION

A. Scanning

The scanning of the 60 000 pictures obtained in the experiment requires two operations:

(a) a selection of the pictures;
(b) for the selected pictures, the measurement of spark coordinates and the computation of the parameters of the proton tracks.

(*a*) *Selection of the Pictures*

In a good picture, we must see the proton track in both views of each spark chamber.

The pictures will be measured if there is one track and one track only in each chamber. There are few pictures with no track in the small chambers but about 30% of the pictures show no track in the big chamber CH4: a proton can be scattered outside this chamber or can be lost by nuclear reactions in the counter SC4 or in the copper plate in front of the chamber. There are also about 15% of the pictures showing more than one track in the chambers. One of the tracks comes from a normally scattered proton but the other belongs to a background particle or to an unscattered proton coming, before the triggering pulse, during the chamber sensitive time. As we cannot follow a track from one chamber to another, these pictures must be discarded.

It would be helpful to reject pictures corresponding to an inelastic carbon scattering with a carbon excitation energy greater than 10 MeV, since the analyzing power is not the same for the carbon levels at excitation energies of 15 MeV or more as for the levels excited at less than 15 MeV. We would deduce the carbon excitation energy from the range measurement performed in the big chamber CH4. But we have found during data analysis that some gaps of chamber CH4 had a relatively small sparking efficiency (70%). This gives an error on the measured range of some protons and an error on the carbon excitation energy. We have found also that the inefficiency of some gaps varies from one place to another. If we do not put a limit on the carbon excitation energy this inefficiency does not introduce any bias into the polarization measurement, as we required to see at least two sparks for the tracks going beyond the third gap in chamber CH4, and as the probability of seeing less than two sparks under these conditions is extremely small. But if we put a limit on the carbon excitation energy, some events would be rejected wrongly by gap inefficiency and if this varies from one place to another a bias would be produced.

In order to remove this bias and to reduce the number of events giving an inelasticity of more than 10 MeV, we reject events in which the proton stops before the fourth gap of the chamber CH4. Eighteen percent of the pictures are excluded by this criterion.

In Fig. 8, we see that the number of events with an inelasticity of 15 MeV or more is less than 6%. In the histogram, the computed inelasticity may be larger than the real one because if a proton does not give a spark in the last gap of its range, its computed energy will be less than its real one.

As the fourth gap had a very small inefficiency and as only a few protons stop in the plate just behind, this procedure gives a very small bias.

[16] R. F. Stiening, E. Loh, and M. Deutsch, Phys. Rev. Letters **10**, 536 (1963).

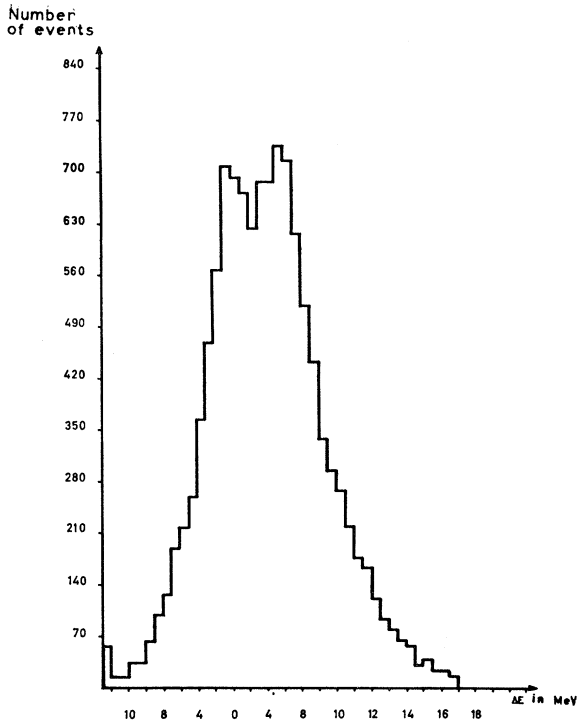

FIG. 8. Histogram of the recoiling C^{12} excitation energy ΔE.

The rules for discarding a picture before the measurement are then (1) no track in one spark chamber; (2) more than one track in one spark chamber; (3) a track stopping before the 4th gap of the big chamber CH4.

(*b*) *Measurement of the Pictures*

In every film we measured the selected pictures and also pictures of the 5 fiducial marks. On these we measured the coordinates on the film of the images of the 5 fiducial marks for each spark-chamber view. As we have seen, this is enough to determine the relation between the coordinates of a spark track point with respect to fiducial marks and the coordinate of its image on the film. About ten pictures of the 5 fiducial marks were measured on each film in order to reduce the measurement errors.

On the selected pictures we measured on each spark-chamber view the coordinates of the images A and B of the two fiducial marks, and the coordinate of the track-point image located in the median plane of each chamber's first gap. From these measurements we computed the coordinates x, y of that point with respect to a reference system bound to the spark chamber.

As the position of the chamber's fiducial marks had been measured we deduced the coordinates of the four points (one in each spark chamber) in the laboratory system.

As a check we measured also for each view the angle between the proton track and the bisector of the images of the AA1 and BB1 lines (Fig. 6). This determines the proton track direction projected on each view and will be only used as a check.

Then we computed the parameters of the track:

(1) The angle θ between the proton track before the carbon block and its track after the carbon block (Fig. 9) which is approximately the scattering angle. The small difference is due to multiple scattering.

(2) The angle ϕ between the vertical direction and the normal to a plane parallel to these two tracks. This plane is also approximately the scattering plane. Polarization of the protons would result in an asymmetry in the observed values of ϕ.

(3) The scattering point in the carbon block.

(4) The minimum distance ρ between the two tracks. The smallness of ρ is a check on the coplanarity of the two tracks.

(5) The limits ϕ_1 and ϕ_2 of the possible angles ϕ. For some scatter points and scattering angles θ, not all values of ϕ can be observed in pictures because there are some values of ϕ which correspond to a scattered proton track, passing either outside the counter SC4 or inside the anticoincidence counter SC5. The observable values of ϕ in these pictures are thus limited to an arc (ϕ_1, ϕ_2). An error on the position of the counters SC4 and SC5 introduces an error on the limits ϕ_1 and ϕ_2 and we get a false asymmetry in the observed ϕ values. In order to suppress such an asymmetry in the computation of ϕ_1 and ϕ_2 the counter SC4 was replaced in the calculations by a larger imaginary counter and the counter SC5 by a smaller imaginary counter.

(6) The energy W of the protons if its scattering angle in the target had been exactly 40.3°. W is computed by taking the intersection of the track with the focal plane "with compensation."

(7) The scattering energy E of the proton on the carbon nucleus. E is obtained by the intersection of the proton track with the focal plane "without compensation" and by taking account of the energy loss in carbon before scattering.

(8) The inelasticity ΔE of the carbon scattering. ΔE is computed from E and the proton range after the carbon scattering.

(9) $\Delta\alpha_1$ to $\Delta\alpha_8$. $\Delta\alpha_j$ is the angle between the projection of the computed proton track and the measured direction in the jth view. The computed track is the

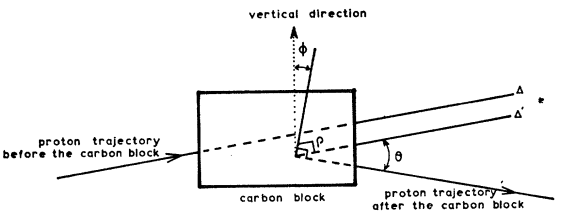

FIG. 9. Geometrical representation of the track parameters. The line Δ' is parallel to the proton trajectory Δ before the carbon block.

one calculated from the coordinates of the two points in two successive spark chambers. On the other hand the direction in the jth view was independently measured in the scanning as we have seen before.

The measurements were done with a scanning table purchased from the Société Française des Appareillages de Télécommandes connected to a read-in–read-out 026 puncher from IBM. The projected pictures were nearly as big as the chambers. The resolution was 0.1 mm in X and $\pi/1000$ rad for the angle. The linearity in X was better than 0.1 mm/1 m. The 22 000 pictures gave 110 000 punched cards (5 per event). The reconstruction of the event was done with the UNIVAC 1107 of the Faculté des Sciences d'Orsay. The results were registered on a magnetic tape which was used as input for the polarization computation program.

B. Polarization Computation

The program is divided in two parts:

(a) a second selection of the events from the parameters of the track in order to reject bad events;
(b) the estimation of the polarization.

(a) *Selection of the Events*

We give here the criteria for successive rejections.

(1) *Rejection of an event in which one of the* $\Delta\alpha$ *is bigger than a limit* $\Delta\alpha_0$. Figure 10 shows the histogram of one of the 8 obtained angles $\Delta\alpha$. In the neighborhood of 0 the distribution is Gaussian and is due essentially to the error in measuring the tracks. The average of $\Delta\alpha$ would be zero if there were no bias in the scanning. In fact the average $\Delta\alpha$ is only 3×10^{-3} rad, that is, 0.1 mm on the coordinates of a point or 0.1 mm on the relative position of A and A1. We choose $\Delta\alpha_0=5\sigma$, where σ is the standard deviation of the distribution: 4600 events are so rejected. Sixty percent of the rejected events come from a $\Delta\alpha$ in the third chamber. They are caused by protons scattering in that spark chamber or in the counter SC4.

(2) *Rejection of an event with a* ρ *bigger than 15 mm.* Figure 11 gives the distribution in ρ. Near 0 it is a normal distribution with a 4-mm standard deviation. This distribution is due essentially to multiple scattering in carbon.

The events with ρ bigger than 15 mm correspond to an error in scanning or to plural scattering in the carbon block. Five hundred events were rejected in this way.

(3) *Rejection of events with a* W *outside the range 318–329 MeV.* Figure 12 shows the distribution in W. SC1 selects the events with W in the range 318–329 MeV. Five events were outside this range and rejected.

(4) *Rejection of events with a scattering angle in carbon less than 8°.* Figure 13 shows the distribution in θ. There is a maximum at $\theta=10°$. The cross section decreases with increasing θ and, on the other hand, almost all the events with $\theta<10°$ trigger the anticoincidence counter SC5 and are not registered.

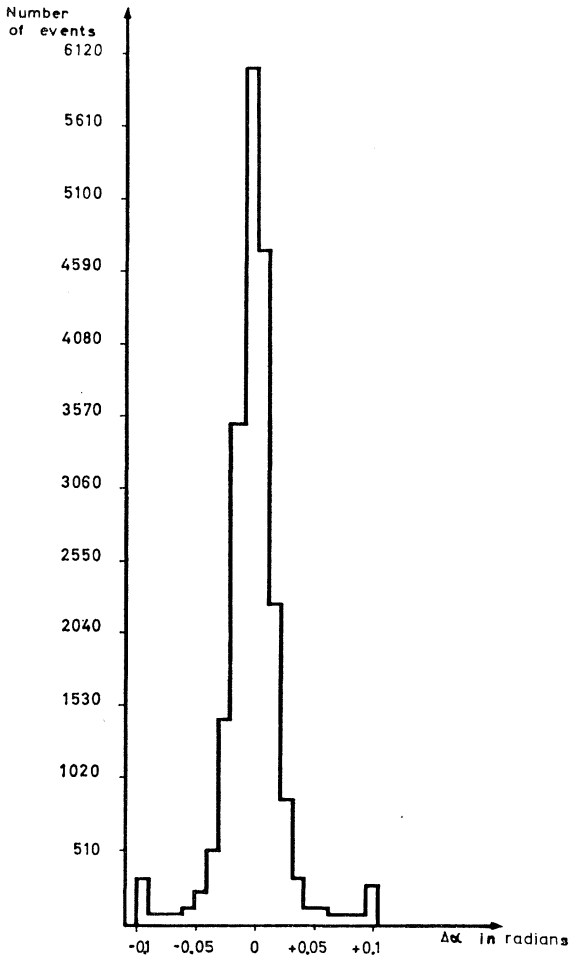

FIG. 10. Histogram of one $\Delta\alpha$ angle.

We reject the events with $\theta<8°$ because the analyzing power of the carbon is poorly determined in this range since multiple and plural scattering introduce error in its computation: thus 2200 events are rejected.

(5) *Rejection of events scattered outside the carbon block.* Figure 14 shows the distribution of the abscissas of the scattering point. We reject 2500 events scattered outside the carbon block (in the plates of a spark chamber or in a counter).

(6) *Rejection of events for which the observable values of* ϕ *are limited by the two imaginary counters.* We have seen (Sec. IV A) that there are two imaginary counters replacing the coincidence counter SC4 and the anticoincidence counter SC5. It may happen for some incident tracks, scattering points and scattering angles θ that the observable values of the ϕ angle were limited by one of these two imaginary counters. It may also happen that these values are limited by both imaginary counters. For computational convenience we reject these 1500 events.

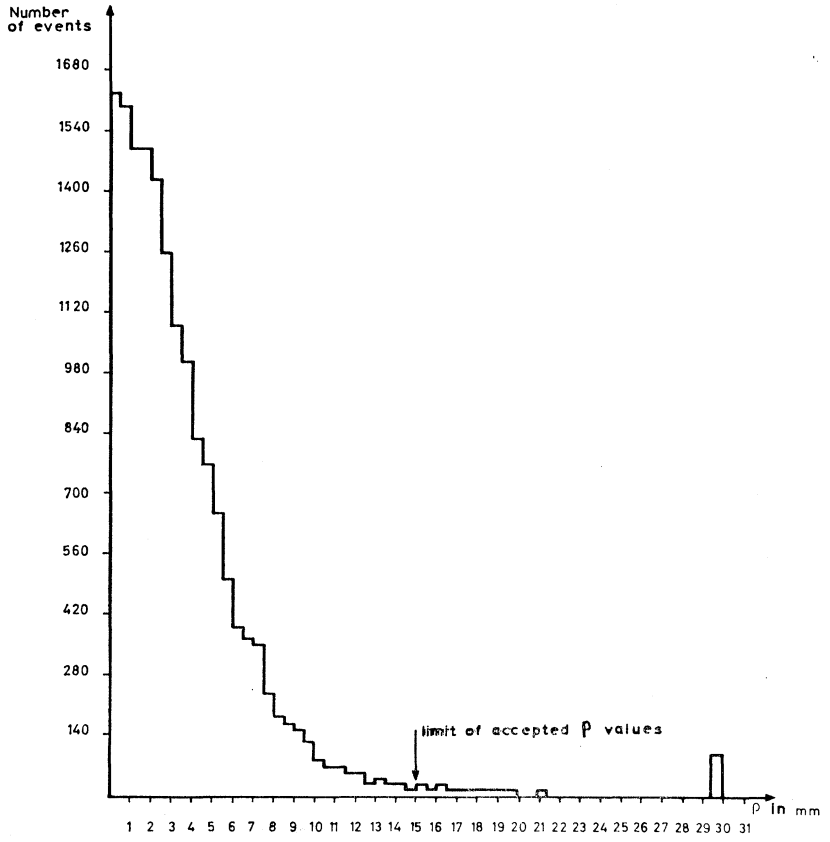

FIG. 11. Histogram of the minimum distance ρ between the proton trajectories before and after the carbon block.

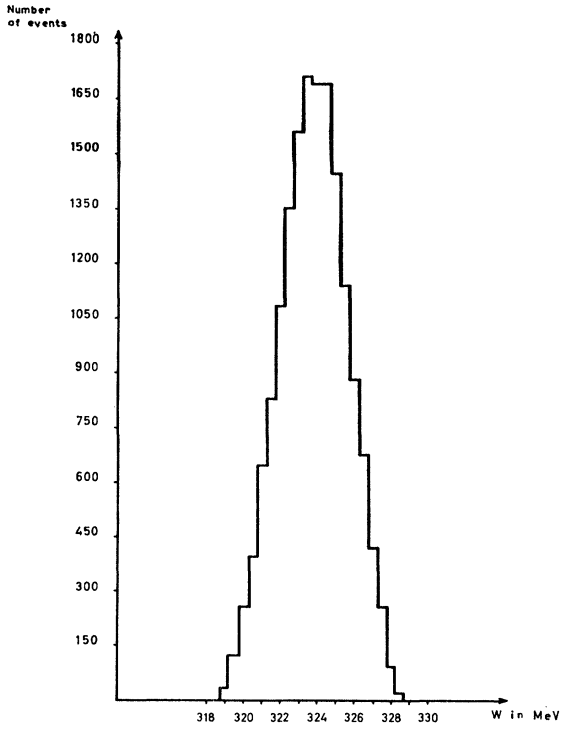

FIG. 12. Histogram of the energy W corresponding to a 40.3° scattering angle in the H_2 target.

(b) *Polarization Computation*

There are 9223 nonrejected events out of the 22 000 measured ones. Of these, 5083 events have ϕ values not limited by any imaginary counter (we call them "complete-arc" events). The other 4140 events have ϕ values limited to an arc (ϕ_1, ϕ_2) by one imaginary counter (we call them "incomplete-arc" events). We can set these two event groups together by putting $\phi_1=0$ and $\phi_2=2\pi$ for the first-group events.

For computing the polarization, we apply the maximum-likelihood method to the analyzed events. The probability density $f_i(\varphi)$ for the azimuthal angle φ of the ith event is

$$f_i(\varphi)=\frac{1+A_i(X\sin\varphi+Y\cos\varphi)}{2\omega_i[1+A_i\eta_i(X\sin\psi_i+Y\cos\psi_i)]},$$

where A_i is the analyzing power for the ith event, X and Y are the values of the horizontal and vertical components of the transverse polarization,

$$\omega_i=\tfrac{1}{2}(\varphi_2-\varphi_1) \quad \text{for the } i\text{th event},$$
$$\psi_i=\tfrac{1}{2}(\varphi_1+\varphi_2) \quad \text{for the } i\text{th event},$$
$$\eta_i=(\sin\omega_i)/\omega_i.$$

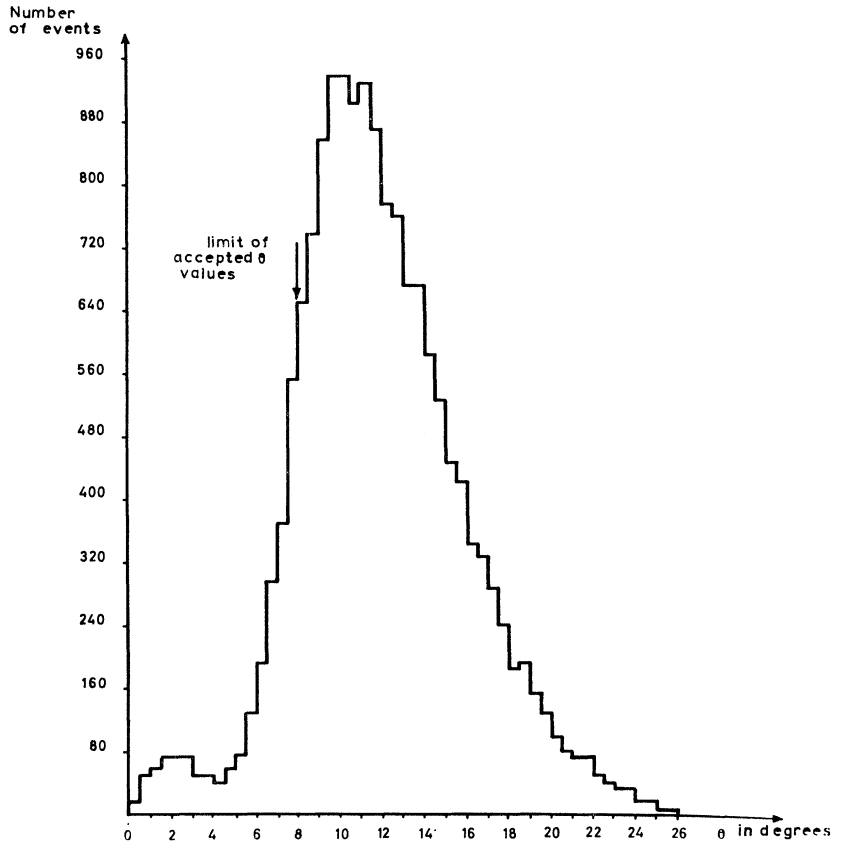

FIG. 13. Histogram of the angle θ between the proton trajectories before and after the carbon block.

The maximum-likelihood method gives

$$\sum_{i=1}^{N}\left[\frac{A_i\sin\varphi_i}{1+A_i(X\sin\varphi_i+Y\cos\varphi_i)}-\frac{A_i\eta_i\sin\psi_i}{1+A_i\eta_i(X\sin\psi_i+Y\cos\psi_i)}\right]=0,$$

$$\sum_{i=1}^{N}\left[\frac{A_i\cos\varphi_i}{1+A_i(X\sin\varphi_i+Y\cos\varphi_i)}-\frac{A_i\eta_i\cos\psi_i}{1+A_i\eta_i(X\sin\psi_i+Y\cos\psi_i)}\right]=0.$$

We then make two approximations:

(1) We take the power series of both equations up to the first order in X and Y, getting

$$X\sum_i A_i^2(\sin^2\varphi_i-\eta_i^2\sin^2\psi_i)+Y\sum_i A_i^2(\sin\varphi_i\cos\varphi_i-\eta_i^2\sin\psi_i\cos\psi_i)=\sum_i A_i(\sin\varphi_i-\eta_i\sin\psi_i),$$

$$X\sum_i A_i^2(\sin\varphi_i\cos\varphi_i-\eta_i^2\sin\psi_i\cos\psi_i)+Y\sum_i A_i^2(\cos^2\varphi_i-\eta_i^2\cos^2\psi_i)=\sum_i A_i(\cos\varphi_i-\eta_i\cos\psi_i).$$

(2) We replace the coefficients of X and Y by their expectation value in the zeroth order in X and Y, obtaining

$$aX+bY=\sum_i A_i(\sin\varphi_i-\eta_i\sin\psi_i),$$
$$bX+cY=\sum_i A_i(\cos\varphi_i-\eta_i\cos\psi_i),$$

with

$$a=\tfrac{1}{2}\sum_i A_i^2(\lambda_i-\mu_i\cos2\psi_i),$$
$$b=\tfrac{1}{2}\sum_i A_i^2\mu_i\sin2\psi_i,$$
$$c=\tfrac{1}{2}\sum_i A_i^2(\lambda_i+\mu_i\cos2\psi_i),$$
$$\lambda_i=1-\eta_i^2,$$
$$\mu_i=\eta_i\cos\omega_i-\eta_i^2.$$

The second approximation allows us to compute the bias of the estimation and its standard deviation. The bias is of second order in X and Y.

We find

$$X=0.000,\quad Y=0.040.$$

The sign is given according to the Basel convention[17]; P is defined positive in the sense of the vector

$$\mathbf{n}=\mathbf{k}_e\times\mathbf{k}_p/|\mathbf{k}_e\times\mathbf{k}_p|,$$

[17] *Proceedings of the International Symposium on Polarization Phenomena of Nucleons, Basel, 1960*, edited by P. Huber and K. P. Meyer [Helv. Phys. Acta Suppl. **6**, (1961)].

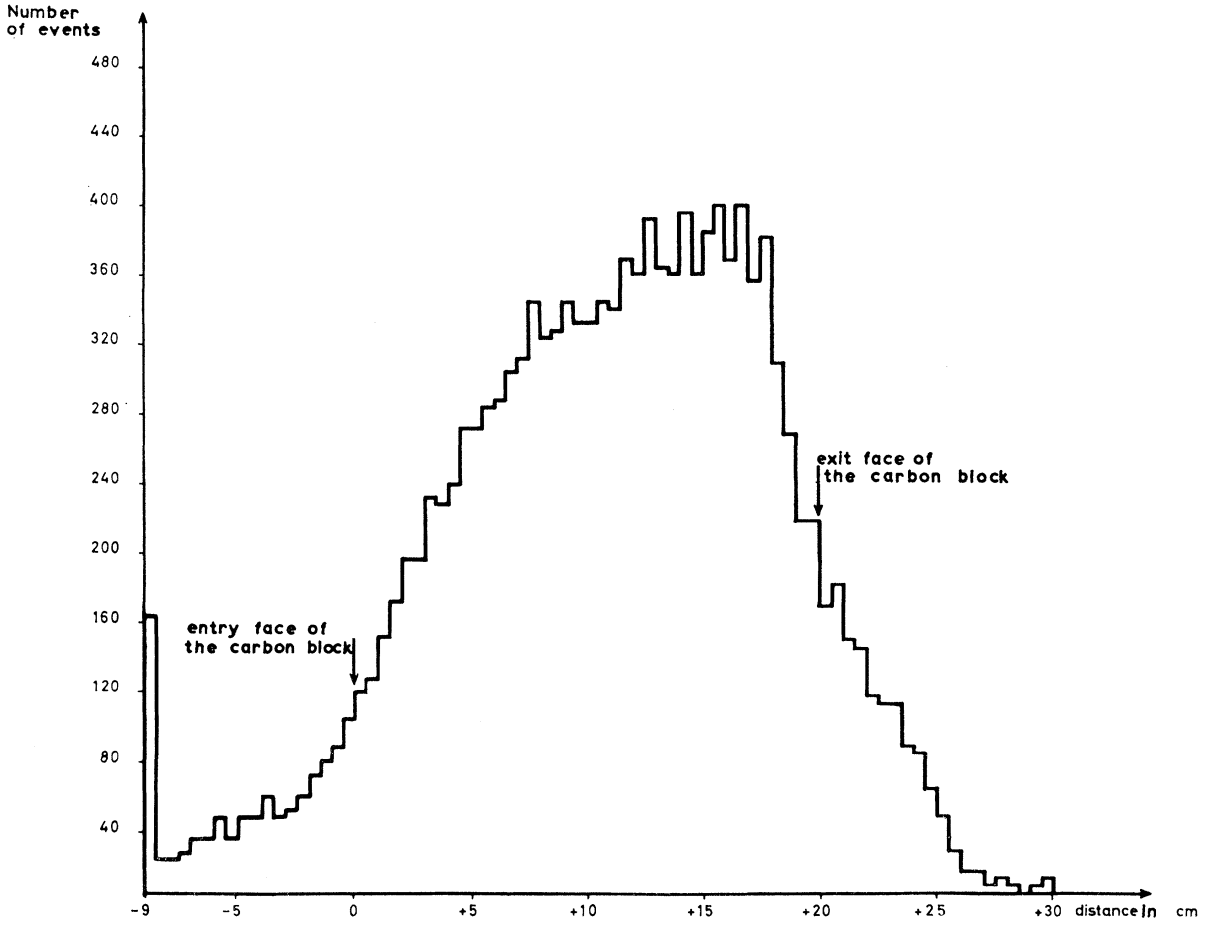

FIG. 14. Histogram of the scattering-point abscissa in the carbon block.

where $\mathbf{k}_e$ and $\mathbf{k}_p$ are the momenta of the incident electron and recoil proton, respectively.

C. Error Estimation

(a) *Statistical Error*

This is the standard deviation computed from the method of estimation: we find that to the zeroth order in X and Y, we have

$$\sigma^2(X)=c/(ac-b^2), \quad \sigma^2(Y)=a/(ac-b^2).$$

The neglected coefficient of Y in $\sigma^2(Y)$ is very small (it should be zero if we consider only the complete-arc events). We find, then,

$$\sigma^2(X)=0.021, \quad \sigma^2(Y)=0.021.$$

(b) *Error in the Analyzing Power*

There are three sources of error:

(1) The error assigned to A_i in the analyzing power tables of Peterson[18]; we took

$$\Delta A/A\sim 5\%.$$

(2) The error in measuring θ due to multiple scattering in the carbon block. We obtain

$$\Delta A/A\sim 5\% \quad (8\% \text{ for } \theta\sim 8^\circ,\ 4\% \text{ for } \theta\sim 11^\circ).$$

(3) The error coming from the events in which the carbon nucleus is left in an excited level higher than 10 MeV. We saw that we had less than 6% of such events. As the absolute error is of the order of 0.1 for these events, we get, then, on the whole, $\Delta A/A=0.9\%$.

Adding these three errors quadratically, we get:

$$\Delta A/A=7\%.$$

Taking $Y=0.04$, we get from this error

$$\Delta Y=0.003.$$

[18] V. Z. Peterson, University of California Radiation Laboratory Report No. UCRL-10622, 1963 (unpublished).

(c) "False Asymmetry" Errors

They come from an error in the measurement of a parameter of the proton tracks. More precisely, the false asymmetry comes from the fact that some events are improperly rejected or analyzed. In order to produce a false asymmetry, the error must depend on the azimuthal angle φ.

(1) *Error on the coordinates of a point of the track.* We must take into account only the systematic error. The sources of error are:

(a) Errors in measuring the relative position of the fiducial marks drawn on the chambers: less than 0.05 mm.

(b) Errors in measuring the chamber positions in the laboratory system: less than 0.05 mm.

(c) Errors coming from the optical aberrations: we found that the coordinates of the picture of a high-precision ruler verify a homographic relation with an error less than 0.1 mm.

(d) Errors in picture scanning: A film was scanned independently by different persons and we computed the distribution of the difference between the two scannings. Table III gives the mean and the standard deviation of these differences for both coordinates X and Y of the four chambers. As there were 20 scanners we think that the final error is less than 0.1 mm.

(e) Errors coming from the thermal expansion of the chambers: We corrected the expansion of chamber CH4; the error due to the expansions of the little chambers is of the order of 0.1 mm for a variation of 10°C. As these 5 errors are independent, we may add them quadratically and we obtain 0.2 mm for the errors on the X and Y coordinates. For the Z coordinate the error is due essentially to the measurement of the position of the chambers. It is about 5 mm.

In order to estimate the resulting error on the polarization, we computed the polarization for a fictitious displacement of the chambers of 0.2 mm in OX or 0.2 mm in OY or 5 mm in OZ. Doing this computation successively for the three coordinates of the four chambers and adding the resulting deviations quadratically, we found that the error on the X and Y components of the polarization due to an error in the coordinates is 0.0146.

(2) *Errors on the position of the imaginary counters.* The effect of imaginary counters must be more severe than the effect of the real ones in rejecting events: We must make sure that an event rejected by a physical counter will have been, *a fortiori*, rejected by the imaginary one. But the imaginary counter must not be too different from the physical one if we do not want to lose too many good pictures. Two checks were used to verify the accuracy of the fictitious counter position:

(a) We made maps of the events in the planes of the fictitious counters in order to see that they did intersect the real counters (Figs. 15 and 16).

(b) We computed the polarization for a displaced imaginary counter. As long as it does not intersect a physical one, the computed polarization does not vary, but the number of analyzed events does, appreciably. On the contrary, when the imaginary counter cuts the physical one, the polarization varies very much but the number of analyzed events in nearly constant (Fig. 17). We estimate the error corresponding to the fictitious counter position to be less than 0.003.

(3) *Error due to an inefficiency of the physical counter SC4.* We saw that the efficiency of SC4 is better than 0.997. As we have always tested this efficiency, we can tell that the polarization error from this source is less than 0.006.

(4) *Error due to an inefficiency of the 4th gap of the chamber CH4.* We measured the inefficiency of this gap for protons stopping behind it, we found $98.3\%\pm0.1\%$. We measured also the asymmetry of the inefficiency with respect to the vertical median plane of the chamber; we found -0.060 ± 0.082 instead of -0.088 ± 0.084 computed from the value of the Y polarization. The asymmetry caused by the inefficiency of the fourth gap is then -0.0015 ± 0.0014. As there are only 8% of the events which stop in the fourth gap, the correction due to the Y polarization is -0.0002 ± 0.0002; we neglected the correction. It would be greater for the X polarization: -0.001 ± 0.0002. We neglected it also and took account only of the corresponding error: 0.001.

(5) *Error coming from the selection of the pictures.* A bias may be introduced by the scanning selection of pictures. In order to reduce and test this bias the

TABLE II. Coincidence counting rates.

Coincidence	Counting rate (per sec)
12	9
34	3.7
$1234\bar{5}$	0.45
12345 with dead time of the camera	0.25

TABLE III. Average and standard deviation of the difference between two measurements of four points X and Y coordinates, one point in each of the 4 spark chambers CH1 to CH4. These two measurements were obtained by two different scannings of the same film made by two different persons.

	X		Y	
Chamber	Average (mm)	Standard deviation (mm)	Average (mm)	Standard deviation (mm)
CH1	0.06	0.35	0.24	0.36
CH2	0.11	0.31	0.06	0.36
CH3	0.11	0.73	0.15	0.78
CH4	−0.05	0.74	0.05	0.70

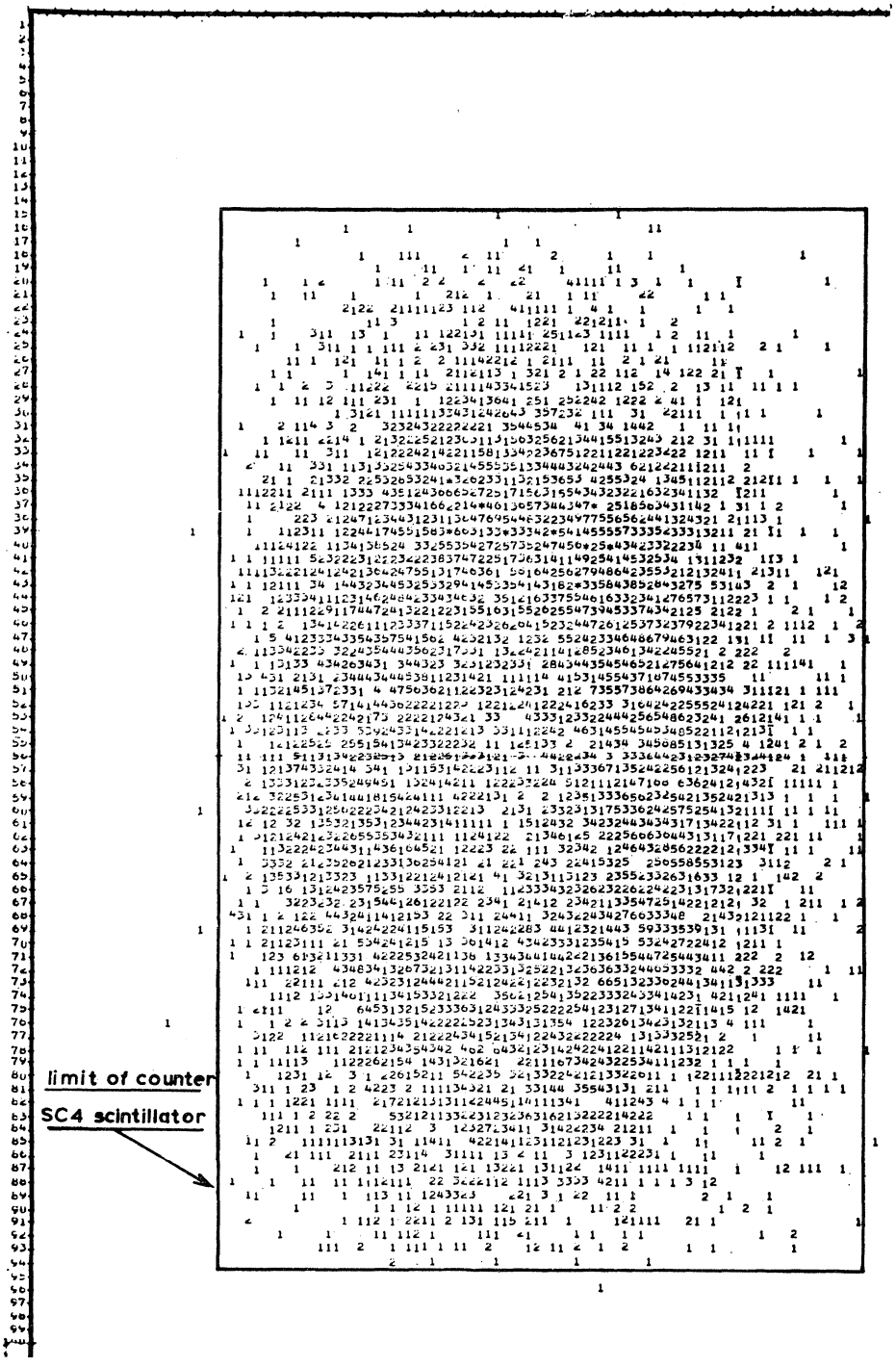

FIG. 15. Map of events in the counter SC4 scintillator. Each point represents events situated within a 2×2 mm^2 square.

selection was done twice by different operators. Then we estimated the error introduced to be less than 0.001.

(*6*) *Error coming from the rejection of events in* $\Delta\alpha$. To reduce this error, we scanned once more the events rejected in this way. We estimated the error to be less than 0.002.

Table IV shows the estimated values of the different "false asymmetry" errors. Adding quadratically all these errors, we find 0.0165 for the Y component of the polarization and 0.018 for the X component.

(*d*) *Parasite Particles*

To these three computed errors we must add a fourth one coming from the omission of some corrections to the

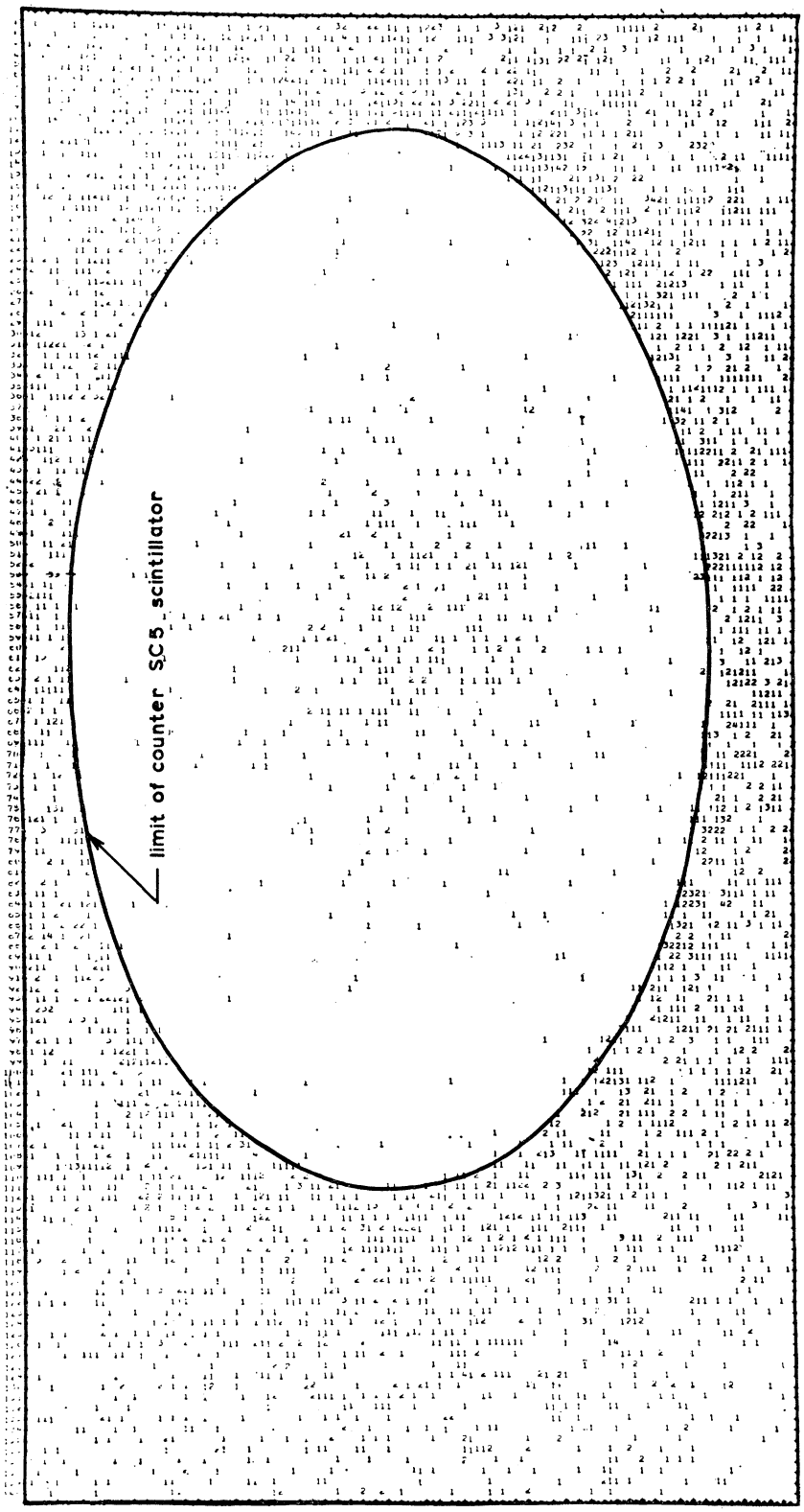

FIG. 16. Map of events around the counter SC5 scintillator.

TABLE IV. Bias on the polarization component Y from different "false asymmetries."

(1) Error on the coordinates of the track points:	0.015
(2) Error on the position of the imaginary counters:	0.003
(3) Inefficiency of the physical counter SC4:	0.006
(4) Inefficiency of the chamber CH3:	0.003
(5) Error due to the selection of pictures:	0.001
(6) Error due to the rejection of events in $\Delta\alpha$:	0.002

value of the Y component of the polarization. Indeed in the proton beam there are few particles which do not come from an elastic scattering e-p. These are:

(a) Particles which did not come from the hydrogen in the target. They contributed $0.3\%\pm0.07\%$ of the total counting rate.

(b) Recoil protons in Compton scattering; $\gamma+p\rightarrow\gamma+p$. We saw that we had less than 0.15% of such particles.

(c) Recoil protons from photo- or electroproduction of π^0 on hydrogen. We estimated that we had about 0.1% of such particles.

(d) "Ghost" protons, approximately 0.5%.

We cannot compute the corrections to the Y component of the polarization due to particles (a)–(d), as we did not measure their polarization. Thus we considered them as errors and we added the different errors quadratically, obtaining 0.006.

When we added quadratically all the errors we obtained the total error on the X and Y components of the polarization 0.027 for the Y component and 0.028 for the X component.

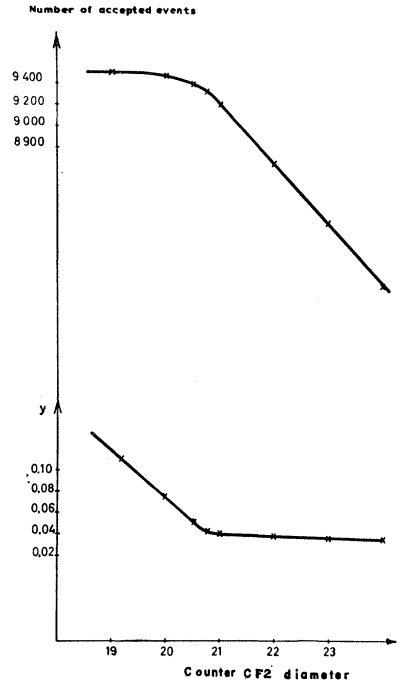

FIG. 17. Polarization component Y and the number of accepted versus the counter CF2 diameter.

(e) χ^2 Tests

We divided the 9223 analyzed events in different groups according to the value of one computed parameter of the tracks, and we checked the reproducibility of the polarization as a function of these parameters by a χ^2 test. By doing so for every parameter, excluding of course the azimuthal angle of carbon scattering, we obtained Table V. All the tests may be considered as satisfactory except the $\varphi_1-\varphi_2\chi^2$ test.

TABLE V. Table of the values of the χ^2 function.

Parameter	X component χ_x^2	$P(\chi^2>\chi_x^2)$	Y component χ_y^2	$P(\chi^2>\chi_y^2)$	Degrees of freedom
ρ	10.78	0.45	13.90	0.18	10
W	6.32	0.60	4.38	0.85	8
θ	10.62	0.10	6.14	0.40	6
Abscissa Z of the scattering point	0.72	0.95	4.95	0.25	4
ϕ_1-ϕ_2	0.95	0.30	5.45	0.02	1
Scanner	21.65	0.50	13.65	0.92	22
Film	32.64	0.32	25.12	0.70	20

We divided the events into two groups: "complete arcs" and "incomplete arcs"; we found 0.003 ± 0.027 for the first group and 0.110 ± 0.037 for the second group, with a χ^2 corresponding to a probability of 2%.

We must first notice that in computing $14\chi^2$, the probability of finding one of them corresponding to a probability less than p is

$$q=1-(1-p)^{14};$$

that is, for $p=0.02$, $q=0.25$.

But as this is not enough to rule out the possibility of a systematic error, we made some more tests.

We calculated, for instance, the polarization by varying the radius of the imaginary counter. We calculated also the polarization for events which are in the neighborhood of the limit between the "complete-arc" group and the "incomplete-arc" group. We checked also that the "complete-arc" events were as sensitive as the incomplete ones to any false asymmetry bias—for example, to a chamber-alignment error. We calculated also the polarization of these two events' groups displacing artificially a chamber by 2 mm.

All these tests were negative. As we can exclude an error in the program (the polarization of a group of "complete-arc" events does not vary if we transform them artificially into "incomplete-arc"), we can say that the probability of a systematic error is very small and we conclude that the discrepancy was purely statistical.

ACKNOWLEDGMENTS

We thank Professor A. Blanc-Lapierre for extending to us the facilities of the laboratory. We are greatly

indebted to Dr. J. K. Walker for his invaluable collaboration in the first stages of the experiment. We express our gratitude to Dr. B. Milman for his help in setting up the experiment. We are grateful to V. Round and his collaborators for building the experimental equipment, to B. Boutouyrie and the magnet group, to the electronics group, to L. Burnod and J. Verlon and the machine crew. We thank Professor M. Gourdin for useful discussions and for clarification of theoretical points. We acknowledge the help, during the runs, of B. Delcourt and Dr. P. Bounin, Dr. D. Frèrejacque, Dr. Nguyen Ngoc and R. Riskalla. Finally, we wish to thank J. Jeanjean and J. Ortega for their valuable collaboration.

PHYSICAL REVIEW VOLUME 140, NUMBER 5B 6 DECEMBER 1965

Some Consequences of the Proposed C and T Violations in Electromagnetic Interactions*

G. FEINBERG
Department of Physics, Columbia University, New York, New York
(Received 19 July 1965)

The model in which C and T are violated in the electromagnetic interactions of hadrons is considered further. It is shown that in this model, the nucleons should have electric dipole moments of order 10^{-19} cm$\times e$, comparable to the present upper limit for the neutron electric dipole moment. The effect of mixing between η^0 and $X^0(960)$ on the decays $\eta^0 \to \pi^0 e^+ e^-$, $X^0 \to \pi^0 e^+ e^-$, and $X^0 \to \eta^0 e^+ e^-$ is discussed, and some estimates for the branching ratios are presented. It is found that the branching ratios of these to all η^0 and X^0 decays may be about 1%.

I. INTRODUCTION

RECENTLY[1] it has been proposed that the CP-violating decay[2] $K_2 \to 2\pi$ occurs through a combination of the CP-conserving weak interaction, and a P-conserving, CP-violating term in the electromagnetic interaction of the hadrons. In this paper, some consequences of this model are pointed out. These concern the electric dipole moments of the baryons, and some of the proposed direct tests of the C-violating electromagnetic interaction. The first of these points involves only the assumption that the source of the CP violation is electromagnetic. On the other hand, the analysis of electromagnetic decays of hadrons involves some assumptions about the $SU(3)$ transformation properties[3] of the $C=+1$ electromagnetic current K_μ. Some remarks are also made about ways to distinguish electromagnetic C violations from strong C violations.

II. ELECTRIC DIPOLE MOMENT OF BARYONS

The existence of an electric dipole moment (EDM) for the neutron or proton would be an indication of CP violation for some interaction. It has been pointed out[4] that such a dipole moment could be generated by a weak, CP-violating, $\Delta S=0$, four-baryon interaction. In the presence of such an interaction, one would expect the EDM of a nucleon to be approximately

$$d \simeq e G_F m_p \sin\theta \simeq (10^{-19} \sin\theta)\ \text{cm}\times e, \qquad (1)$$

where $\sin\theta$ is a phase angle measuring the CP violation in weak interactions. In the absence of a detailed dynamical argument to the contrary, one considers the small magnitude of the ratio $(K_2 \to 2\pi)/K_1 \to 2\pi)$ as indicative of the size of $\sin\theta$. Then one would expect that if the CP violation is an intrinsically weak interaction

$$\sin\theta \lesssim 10^{-3},$$

and (2)

$$d \lesssim 10^{-22}\ \text{cm}\times e.$$

This conclusion is insensitive to the existence or nonexistence of intermediate bosons.

Suppose,[1] however, that a term K_μ, even under T, occurs in the electromagnetic current of the hadrons. Suppose further that the matrix elements of K_μ are comparable to these of the regular electromagnetic current J_μ. Then provided only that there are weak, P-violating, $\Delta S=0$, four-baryon interactions, as experiment seems to indicate,[5] one would expect the nucleon to get an EDM of order

$$d \simeq e G_F m_p \simeq 10^{-19}\ \text{cm}\times e, \qquad (3)$$

* This work was supported in part by the United States Atomic Energy Commission.

[1] J. Bernstein, G. Feinberg, and T. D. Lee, Phys. Rev. **139**, B1650 (1965).

[2] J. H. Christenson, J. W. Cronin, V. L. Fitch, and R. Turlay, Phys. Rev. Letters **13**, 138 (1964).

[3] T. D. Lee, Phys. Rev. (to be published); N. Cabibbo, Phys. Rev. Letters **14**, 965 (1965).

[4] G. Feinberg and H. S. Mani, Phys. Rev. **137**, B636 (1965).

[5] F. Boehm and E. Kankeleit, Phys. Rev. Letters **14**, 312 (1965).